

Physikalisches Praktikum II im SS 2013

UNIVERSITÄT STUTTGART

Report for experiment

V08: Mößbauer Effect

Helmut Frasch,* Henri Menke[†]

13. Mai 2013

Summary

The Mößbauer effect is a physical phenomenon discovered in 1958 by Rudolf Mößbauer and describes the recoilless nuclear resonance fluorescence.

In this experiment we will discuss the emission spectrum of ^{57}Co and measure several properties of different materials, being ^{57}Fe , $\text{FeSO}_4 \cdot 7\text{H}_2\text{O}$ and $\text{K}_4(\text{Fe}(\text{CN})_6) \cdot 3\text{H}_2\text{O}$. The properties determined are isomeric shifts, magnetic fields at the core, the magnetic moment of an excited state and the electric field gradient.

*hel.f@gmx.de

[†]henrimenke@gmail.com

Contents

1	Basics	3
1.1	Radioactive Decay and γ -Radiation	3
1.1.1	Natural Linewidth in γ -Ray Spectra	3
1.1.2	γ -Spectrum of ^{57}Co	4
1.2	The Mößbauer Effect	5
1.2.1	Debye-Waller Factor	6
1.3	Mößbauer Spectroscopy	6
1.3.1	Hyperfine Splitting	6
1.3.2	Interaction with the Electrical Field of the Shell Electrons	7
1.3.3	Quadrupole Splitting	7
1.3.4	Isomeric Shift	8
1.4	Scintillation Counter	8
2	Analysis	9
2.1	Emission Spectrum of ^{57}Co	9
2.1.1	Analysing the Spectrum	9
2.2	Hyperfine Structure of ^{57}Fe	10
2.2.1	Isomeric Shift	10
2.2.2	Magnetic Field at the Core	11
2.2.3	Magnetic Moment of the Excited State of ^{57}Fe	12
2.2.4	Velocity Calibration of the Mößbauer Spectrometer	12
2.3	Isomeric Shift and Electric Field Gradient in $\text{FeSO}_4 \cdot 7\text{H}_2\text{O}$	13
2.3.1	Isomeric Shift	13
2.3.2	Computing the Electric Field Gradient	14
2.4	Isomeric Shift of $\text{K}_4(\text{Fe}(\text{CN})_6) \cdot 3\text{H}_2\text{O}$	14
2.4.1	Computing the Isomeric Shift	14
3	Summary	16
	List of Figures	17
	List of Tables	17
	References	18

1 Basics and Theoretical Background

1.1 Radioactive Decay and γ -Radiation

All atoms consist of an electron shell and a nucleus, which itself is made up of protons and neutrons. The number of protons in the nucleus is called the atomic number and has a direct effect on the atom's chemical properties. This is why the chemical elements are arranged in order of their atomic number. The sum of the numbers of protons and neutrons is called the mass number. If two atoms have the same atomic number, they are called isotopes. If the mass number is equal for two atoms, they are called isobares. Isotopes only differ in their neutron number. Only very few possible isotopes of a given element have stable nuclei. The rest transform into other elements by nuclear decay. This is always a statistical process and it is found that the number of particles in a radioactive material decays exponentially.

There are three kinds of nuclear decay. They are historically differentiated by the energy of the occurring radiation as α -, β - and γ -decay. Nuclear reactions of all three decay types have been identified by considering conservation laws for energy, momentum, mass and number of elementary particles.

- An atom undergoing α -decay emits an α -particle, which is the nucleus of a ${}^4_2\text{He}$ atom. Due to Heisenberg's uncertainty principle the kinetic energy of the α -particle in the nucleus can be high enough that it tunnels through the potential barrier of the quantum well, which holds the nucleus together.
- In β -decay an electron and an antineutrino are emitted while a neutron of the nucleus is transformed to a proton. Thus the atoms before and after the reaction are isobares. A proton is made of two up and one down quark while the neutron consists of one up and two down quarks. The conversion of up to down quarks is caused by the weak interaction. The inverse process of transforming a proton to a neutron is also possible. In this case a positron and a neutrino are emitted. A similar process to β -decay is electron capture. Here an electron of the s-orbital of the atom is captured by a proton of the nucleus. This also transforms the proton to a neutron while a neutrino is emitted.
- There is no transformation of the nucleus when γ -decay occurs. As γ -rays are actually very high energy photons, only the energy level of the nucleus shifts when emitting the radiation. The energy levels of the nucleons can be theoretically calculated in the nuclear shell model in analogy to the electron shell of the atom.

We see that γ -radiation only occurs when the nucleus is in an energetically higher state. This only happens after α - or β -decay or when the nucleus absorbs a γ -photon itself. The decay of the excited state can also happen by internal conversion. In this process the energy associated with an emitted photon is instead given to one of the shell electrons. This conversion electron is then emitted instead of a photon.

1.1.1 Natural Linewidth in γ -Ray Spectra

Every excited state of an atom has a finite lifetime. The Energy-time uncertainty principle

$$\Delta E \tau \geq \frac{\hbar}{2} \quad (1)$$

relates the mean lifetime τ of a state to the energy uncertainty ΔE that determines the linewidth of the respective state in the emission spectrum. We can define a natural linewidth Γ that corresponds to a energy-time uncertainty of \hbar

$$\Gamma = \frac{\hbar}{\tau}. \quad (2)$$

The probability to find a radioactive isotope in an excited state is proportional to its decay rate. As the decay happens in an exponential fashion the probability density of a wave function Ψ_a obeys the relation

$$|\Psi_a|^2 \propto \exp(-\Gamma t). \quad (3)$$

The connection of Γ to the decay constant of radioactive decay is only a heuristic approach. This however means that the linewidth is influenced by every decay process of the isotope in the excited state, which includes internal conversion.

In order to calculate the curve of the emission spectrum we need the time dependent part of the wave function. Considering the exponential decay and the eigenvalue of the time evolution operator $\exp -i\omega_0 t$ of a time independent hamiltonian we get

$$\Psi_a \propto \exp(\Gamma/2 - i\omega_0)t \quad (4)$$

where ω_0 is the resonance frequency at which a photon is emitted. By applying a fourier transformation we get the wave function $\Psi_a(\omega)$ in frequency space. The Probability distribution is then proportional to

$$|\Psi_a(\omega)|^2 \propto \frac{1}{(\omega - \omega_0)^2 + (\Gamma/2)^2}. \quad (5)$$

This is a lorentz distribution with a FWHM of Γ and its peak at ω_0 . In the case of γ -rays the natural linewidth is usually very small because of a very short half life of the excited state.

1.1.2 γ -Spectrum of ^{57}Co

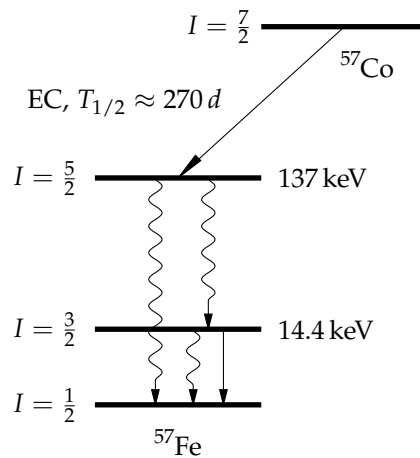


FIGURE 1: Decay of ^{57}Co to the excited state of ^{57}Fe by electron capture. The γ -ray emission at the 14.4 keV level has a probability of about 10%. Other decay processes at that level occur by internal conversion. The transition energies were obtained from [1, p. 44, fig. 4.1]

Mößbauers-spectroscopy utilizes γ -rays with natural linewidth to analyse the structure of isotopes, that can absorb the respective γ -rays. A common isotope used in Mößbauer-spectroscopy is ^{57}Fe . A γ -ray source for this isotope is found in ^{57}Co , which decays to an excited state of ^{57}Fe by electron capture with a half life of about 270 d. The excited state decays in a cascade of γ -rays and internal conversion to the stable ground state. The respective decay scheme is depicted in figure 1. The direct decay from the $I = 5/2$ to the $I = 1/2$ level happens with a 10% probability, whereas I is the nuclear spin quantum number. This transition is an exception to the selection rule $\Delta I = 0, \pm 1$ and is possible because the selection rules are derived with perturbation theory. The partial decay happens in two steps:

- A pure γ -photon decay from $I = 5/2$ to $I = 3/2$ with a probability of 86% and a half life of about 8 ns. The energy of the emitted photon is approximately 122 keV.
- A γ -photon decay from $I = 3/2$ to $I = 1/2$ that happens in 1 of 10 cases. In all other cases the decay is due to internal conversion. The photons of this decay are mostly used for Mößbauer-spectroscopy as the according energy of 14.4 keV allows an easier detection than for the higher energy photons. The half life of this decay is about 100 ns which translates with equation (2) to a natural linewidth of $\Gamma = 4.6$ neV. Since the natural linewidth is caused by all decay types it can be further minimized by a factor of 10 if internal conversion is suppressed.

Emission of other γ -rays with a even lower probability is also possible as seen in [5].

1.2 The Mößbauer Effect

A γ -ray spectrum of a radioactive source usually doesn't show the natural linewidth discussed in the previous section. We can derive this by considering the total energy of the atom before the emission of the photon

$$E(t_1) = E_e + \frac{p^2}{2m} \quad (6)$$

and after the emission

$$E(t_2) = E_g + \frac{(p - \hbar k)^2}{2m}. \quad (7)$$

The eigenenergies E_e and E_g are those of the excited and the ground state respectively. The difference of these energies yields the energy of the γ -rays $E_e - E_g = \hbar\omega_0$. After emission, the momentum $p = mv$ of the atom is changed by the momentum $\hbar k$ of the emitted photon. Thus the actual emission spectrum is described by

$$\omega = \frac{1}{\hbar}(E(t_1) - E(t_2)) = \omega_0 + \mathbf{k} \cdot \mathbf{v} - \frac{k^2}{2m} \quad (8)$$

which includes the doppler broadening $\mathbf{k} \cdot \mathbf{v}$ and the recoil term $\frac{k^2}{2m}$. The emission spectrum is therefore also dependent on the velocity of the atoms. In the case of a gas this means that the spectrum doesn't look like a lorentz distribution but a boltzmann distribution because of the velocity of the single atoms. The mean value of the distribution is shifted by the recoil term. For a more complex structure like a molecule we also have to consider oscillations and rotations with quantized energies of $E_n = \hbar\Omega(n + \frac{1}{2})$ and $E_l = \frac{\hbar^2 l(l+1)}{2\Theta}$ respectively. Here n and l are the quantum numbers of the oscillation and rotation while Ω is the angular frequency of the oscillation and Θ the molecule's moment of inertia. These two kinds of energies can only take on discrete values since the quantum numbers are integers. Upon the emission of γ -rays the molecule can change from a state with quantum numbers n and l to another state with numbers n' and l' which leads to additional energy shifts for the emitted photons. This causes secondary lines in the spectrum of the molecule, which have intensities proportional to the transition probabilities from one eigenstate to another.

For structures of increasing size the total mass increases and leads to a decreasing influence of the recoil term on the spectrum. If we consider a solid, then the mean velocity of each atom is so slow, that the doppler broadening can be neglected, as well. Then the only shift in energy of the emitted γ -rays stems from changes of the lattice oscillations through the eigenstate transitions. In structure with N atoms there are $3N$ possible oscillations, which practically means that there is an infinite number of secondary lines. Because the energy difference $\hbar\Omega$ of adjacent oscillation eigenstates is much smaller than the natural linewidth Γ , this also means a quasi continuous spectrum of the secondary lines.

The Mößbauer effect now states, that the main spectral line at $\omega = \omega_0$ has a much greater intensity than any of the secondary lines. This line is called the Mößbauer line. The probability for a γ -quant to be emitted in the Mößbauer line is expressed by the Debye-Waller factor $f(T)$, which shows a temperature dependency as the intensity of the main line decreases with higher temperatures.

1.2.1 Debye-Waller Factor

The probability of coherent elastic scattering of radiation on a crystal lattice is temperature dependent. This is described by the Debye-Waller factor $f(T)$ which can be expressed as

$$f(T) = \sum_n g(T, n) \cdot w(n, n). \quad (9)$$

This is a sum over all oscillation quantum states n of the lattice where $w(n', n)$ is the probability of transition from the state n' to the state n . As coherent elastic scattering only occurs when the energy state isn't changed, the Debye-Waller factor only considers the n to n transitions. These probabilities are temperature independent because they are only caused by the lattice structure itself. The temperature dependency stems from the general probability $g(T, n)$ to find the oscillation state n at a certain temperature T .

The Mößbauer line contains the coherently elastic scattered γ rays of the spectrum. Thus the Debye-Waller factor can be applied to give a measure of the intensity of this spectral line. The Debye-Waller factor of ^{57}Fe at room temperature is about $f(T) = 0.8$, which means that the Mößbauer line will be clearly visible compared to the rest of the spectrum.

1.3 Mößbauer Spectroscopy

The Mößbauer line can be utilized for high precision spectroscopy of certain materials due to its narrow natural linewidth and high relative intensity. Mößbauer spectra are functions of velocity, as the Doppler effect is used to vary the energy of the Mößbauer line. The emitter and absorber materials have to have a similar energy level structure in terms of the used Mößbauer line because its energy can only be varied slightly before the Mößbauer effect is cancelled out. The doppler effect is introduced by moving the emitter or absorber material in a periodic fashion against each other. The energy E of the γ -rays is then changed by the velocity v according to

$$E = E_0 \left(1 + \frac{v}{c}\right) \quad (10)$$

where c is the speed of light. The sign of v is determined by the direction of the movement of the Mößbauer drive. If it is moving towards the sample, »+« is chosen, otherwise »-«.

The facts described above enable the measurement of small perturbations of the energy level structure of the absorber material relative to the emitter. The perturbations are for example isomeric shift, hyperfine splitting and quadrupole splitting.

1.3.1 Hyperfine Splitting

Every spin induces a magnetic moment in a particle. The interaction of the nuclear magnetic moment μ_I with the magnetic field \mathbf{B} induced by the magnetic moments of the shell electrons creates shifts in the energy structure of an atom or nucleus by $\Delta E = -\mu_I \mathbf{B}$. The nuclear magnetic moment is given by $\mu_I = -g_I \frac{\mu_K}{\hbar} \mathbf{I}$ where \mathbf{I} is the nuclear spin, μ_K the Bohr magneton and g_I the nuclear g-factor. Thus we get

$$\Delta E_m = g_I \frac{\mu_K}{\hbar} \mathbf{I} \cdot \mathbf{B} = g_I \frac{\mu_K}{\hbar} m_I B \quad (11)$$

with the spin quantum number m_I that is an eigenvalue of the spin along the quantization axis given by the direction of B . There are $2I + 1$ possible values for m_I that range from $-I, -I + 1$ to $I - 1, I$. This means that the degenerated energy levels split into $2I + 1$ levels, which are shifted by energy differences of ΔE_m from the degenerated level. This effect is called hyperfine splitting. A photon can be absorbed or emitted for a transition of $\Delta m_I = 0, \pm 1$ as the angular momentum is conserved and the spin of the photons can only take on these three values. In the case of the ^{57}Fe Mößbauer line, which is emitted from the $I = \frac{3}{2}$ state, we get 6 possible energy level transitions.

The hyperfine splitting can be observed as additional lines in the Mößbauer spectrum. A single line source should be used to get the same number of peaks as the number of possible transitions.

1.3.2 Interaction with the Electrical Field of the Shell Electrons

Depending on the electronic configuration of the isotope there can also be an energy level splitting caused by the electric interaction of nucleus and shell electrons. A multipole expansion of the electronic potential gives us

$$\Phi(\mathbf{x}) = \Phi_0 + \sum_{i=1}^3 \left. \frac{\partial \Phi}{\partial x_i} \right|_{x=0} \cdot x_i + \frac{1}{2} \sum_{i,j} \left. \frac{\partial^2 \Phi}{\partial x_i \partial x_j} \right|_{x=0} \cdot x_i x_j + \dots \quad (12)$$

which leads to the interaction potential

$$V = \int \rho \Phi d^3x = eZ\Phi_0 + \sum_{i=1}^3 \left. \frac{\partial \Phi}{\partial x_i} \right|_{x=0} \cdot \int \rho x_i d^3x + \frac{1}{2} \sum_{i,j} \left. \frac{\partial^2 \Phi}{\partial x_i \partial x_j} \right|_{x=0} \cdot \int \rho x_i x_j d^3x. \quad (13)$$

Since the nucleus doesn't have a dipole moment the linear term disappears. Also the constant term will only cause an energy offset that can be added to the energy eigenvalues afterwards. Thus the only significant physical effect is caused by the quadratic quadrupole term. The coefficients $q_{ij} := \left. \frac{\partial^2 \Phi}{\partial x_i \partial x_j} \right|_{x=0}$ make up a symmetrical 3×3 matrix which can be diagonalized so that the quadrupole term reads

$$V_q = \frac{1}{2} \sum_{i=1}^3 q_{ii} \int \rho (x_i^2 - \frac{r^2}{3}) d^3x + \frac{1}{6} \sum_{i=1}^3 q_{ii} \int \rho r^2 d^3x = V_{qs} + V_{is} \quad (14)$$

with $r^2 = \sum x_i^2$. The term V_{qs} describes the quadrupole splitting and V_{is} the isomeric shift. We can furthermore utilize the poisson equation $\Delta \Phi = -4\pi\rho$ to get a general expression for the diagonalized coefficients

$$\sum_{i=1}^3 q_{ii} = (\Delta \Phi)_0 = 4\pi e |\Psi(0)|^2. \quad (15)$$

Here we set the charge density $\rho(0) = -e |\Psi(0)|^2$ of the shell electrons at the nucleus. Hence the wave function Ψ of the electrons is used.

1.3.3 Quadrupole Splitting

The interaction potential of the quadrupole splitting V_{qs} only has an effect on certain geometries of the nucleus or the crystal lattice. A vanishing quadrupole term can be found if the lattice has a cubic structure or if the charge density has spherically symmetric distribution.

We consider the case with $q_{xx} = q_{yy} \neq q_{zz}$, where x, y and z are substituted for the x_i . This corresponds to an ellipsoid charge density. Equation (15) then becomes

$$q_{xx} = q_{yy} = \frac{1}{2} (4\pi e |\Psi(0)|^2 - q_{zz}). \quad (16)$$

We can substitute $q_{zz} = \frac{\partial^2 \Phi}{\partial z^2} \Big|_{x=0} = - \frac{\partial E}{\partial z} \Big|_{x=0}$ and see that q_{zz} is actually the electric field gradient at the nucleus along the z-axis. Inserting this expression in V_{qs} yields

$$V_{qs} = \frac{V_{zz}}{4} \int \rho(3z^2 - r^2) d^3x \quad (17)$$

with $V_{zz} = - \left(\frac{\partial E}{\partial z} \Big|_{x=0} + \frac{4\pi}{3} e |\Psi(0)|^2 \right)$. Thus the expression V_{zz} can be interpreted as the electric field gradient at the nucleus to which also the shell electrons contribute.

The term $(3z^2 - r^2)$ is proportional to the spherical harmonic Y_{20} . This makes it possible to evaluate the integral in terms of the quantum numbers I and m_I and the nuclear quadrupole moment Q . The interaction potential then reads

$$V_{qs} = \frac{eQV_{zz}}{4} \cdot \frac{3m_I^2 - I(I+1)}{3I^2 - I(I+1)}. \quad (18)$$

From this equation we see a splitting of the energy eigenstates in $|m_I|$ components if the charge density has the assumed ellipsoid distribution. This is called quadrupole splitting. The energy difference of these states gives us an information about the electric field gradient V_{zz} if the nuclear quadrupole moment is known.

1.3.4 Isomeric Shift

The Mößbauer spectrum usually isn't symmetrical to $v = 0$. A reason for this is given by different radii of the nucleus in the excited and the ground state. With the mean quadratic nuclear radius in

$$Ze \langle r^2 \rangle := \int \rho r^2 d^3x \quad (19)$$

we get the difference of the V_{is} terms for excited and ground state as

$$V_{is}^e - V_{is}^g = \frac{2\pi}{3} Ze^2 |\Psi(0)|^2 (\langle r^2 \rangle_e - \langle r^2 \rangle_g). \quad (20)$$

Since this effect only depends on the geometry of the nucleus and the electron density at the nucleus it is called the isomeric shift. It can be used to analyse the electron configuration in molecules.

1.4 Scintillation Counter

A scintillation counter is a device for γ -ray detection. Incoming radiation is absorbed or scattered by the atoms of a crystal consisting of the compound NaI doped with thallium. Electrons emitted by the radiation collide with other electrons and lose a constant amount of energy necessary for carrier generation. This process occurs in multiple steps in which a number of electrons proportional to the energy of the radiation is emitted. These electrons are passed on to photo multipliers to get a better signal strength overall.

An advantage of scintillation counters towards geiger counters, which have a better energy resolution, is a better rate of detection due to a greater electron density in a crystal in comparison to a gas.

2 Analysis and Interpretation

2.1 Emission Spectrum of ^{57}Co

Procedure We observe the gamma- and Röntgen-emission spectrum of the cobalt isotope ^{57}Co without any absorber brought into the beam path. The peaks in the spectrum will be identified and described what they mean.

Experimental Setup The absorber-mount is placed in front of the Mößbauer drive. After the absorber-mount a scintillation counter is placed, attached to a photomultiplier and a preamp. The preamp is connected to the main amplifier, which is hooked up to a PC through a data-acquisition module. The data-acquisition module is also connected to the drive unit, where the velocity of the Mößbauer drive can be adjusted. For this first task we toggle absorber-mount such that the beam goes right through it into the scintillation counter. The Mößbauer drive remains turned off.

In figure 2 the measured emission spectrum of the ^{57}Co sample is displayed. In the following we will discuss the peaks, their position and their origin. The peaks are numbered from left to right, which means they are numbered over their energy level. Obviously we will start at [1]:

2.1.1 Analysing the Spectrum

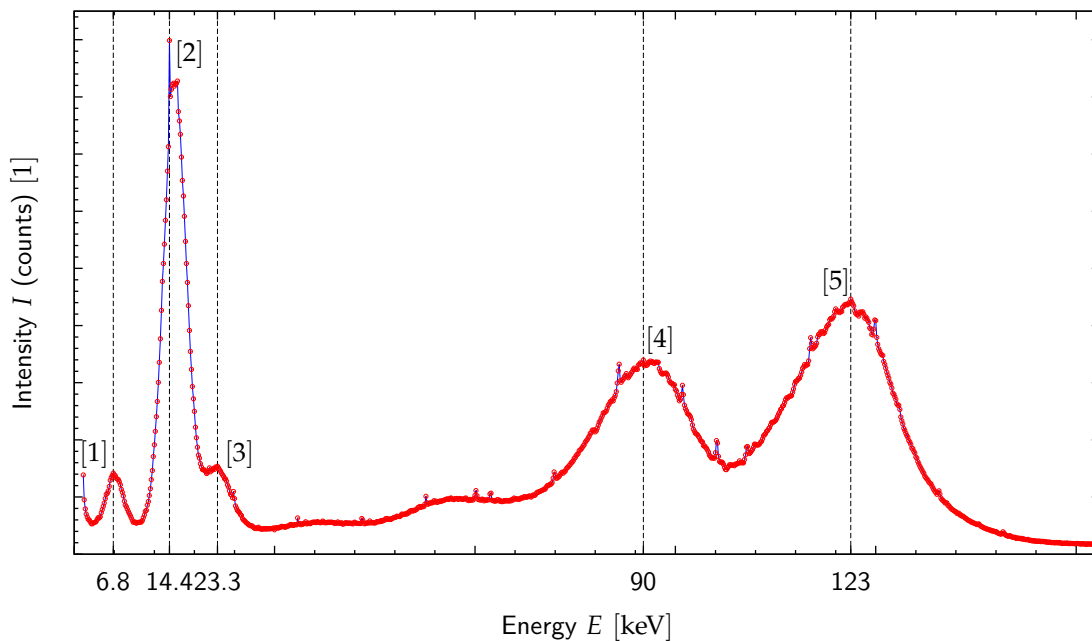


FIGURE 2: Emission spectrum of ^{57}Co .

- [1] This peak is encountered at 6.8 keV and represents the Röntgen emission of the transition of a shell electron to the unoccupied level caused by electron capture.
- [2] At 14.4 keV the Mößbauer-line can be observed which is emitted by the excited ^{57}Fe when it transitions from $I = 3/2$ to $I = 1/2$.
- [3] The ^{57}Co sample is enclosed in rhodium. This rhodium case also emits radiation, in this case at 23.3 keV.

- [4] This peak at about 90 keV is a resonance of the scintillation counter.
 [5] The line at 123 keV is the emission of the transition from $I = 5/2$ to $I = 3/2$.

2.2 Hyperfine Structure of ^{57}Fe

Procedure We are about to determine three properties of ^{57}Fe . First we determine the isomeric shift by observing the shift of the symmetry axis of the emission spectrum around zero velocity. Second we take a look at the magnetic field at the core, therefore we use the equation for the energy level splitting in the hyperfine structure. Third the magnetic moment of the excited state is computed, again using the equation for hyperfine splitting.

Experimental Setup The absorber-mount is placed in front of the Mößbauer drive. After the absorber-mount a scintillation counter is placed, attached to a photomultiplier and a preamp. The preamp is connected to the main amplifier, which is hooked up to a PC through a data-acquisition module. The data-acquisition module is also connected to the drive unit, where the velocity of the Mößbauer drive can be adjusted. For this first task we place a ^{57}Co sample into the absorber-mount and toggle it to place the sample in the beam instead of the lead seal. Then we start the measurement for a period of 30 min with a drive velocity of 9 mm s^{-1} .

2.2.1 Isomeric Shift

The Mößbauer spectrum of ^{57}Fe is displayed in figure 3. When the drive is swinging every velocity occurs twice. That's why half of the peaks had to be mirrored back. The isomeric shift can be calculated from the displacement of the symmetry-axis to the zero-axis. Therefore we take the velocities of very two symmetrical distributed peaks and compute their difference.

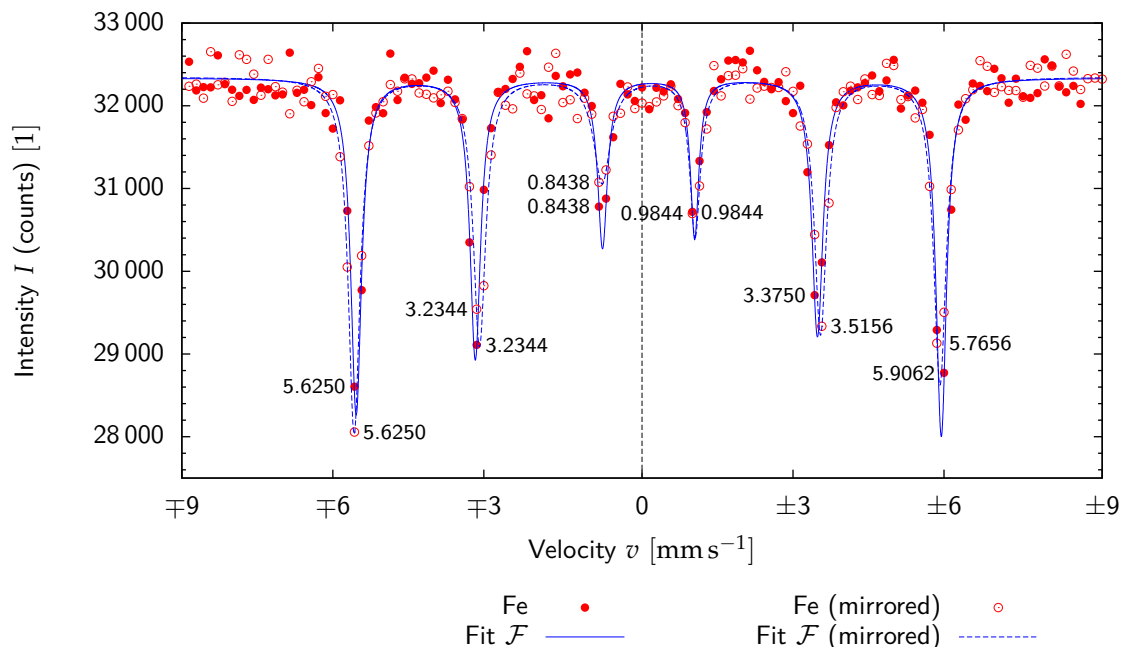


FIGURE 3: Transmission spectrum of elemental iron. The peaks have been annotated with the corresponding velocity of the Mößbauer drive.

The differences are listed in table 1. The arithmetic mean is also listed.

solid line			dashed line		
left side mm s ⁻¹	right side mm s ⁻¹	difference mm s ⁻¹	left side mm s ⁻¹	right side mm s ⁻¹	difference mm s ⁻¹
5.6250	5.9062	0.2812	5.6250	5.7656	0.1406
3.2344	3.3750	0.1406	3.2344	3.5156	0.2812
0.8438	0.9844	0.1406	0.9844	0.8438	0.1406
mean:		0.1875	mean:		0.1875

TABLE 1: Comparison of the differences of the velocities compared between left and right side.

According to these results the mean shift of the zero axis would be 0.1875 mm s⁻¹. Nevertheless this value yields an error, which corresponds to the width of one channel. This width determines the resolution of the velocity of the Mößbauer drive, which is of course finite. We are measuring on 256 channels with a spectrum of -9 mm s⁻¹ to 9 mm s⁻¹, i.e. a width of 18 mm s⁻¹. Because we folded back half of the values, we need to double this width. This results in an error of

$$\frac{2 \cdot 18 \text{ mm s}^{-1}}{256} \approx 0.1406 \text{ mm s}^{-1}$$

That means our shift of the zero axis is determined as

$$\Delta v = 0.1875 \pm 0.1406 \text{ mm s}^{-1}$$

To compute the isomeric shift we need to plug this result into the following equation. We get

$$\Delta E = E_0 \frac{\Delta v}{c} = 14.4 \text{ keV} \frac{0.1875 \text{ mm s}^{-1} \pm 0.1406 \text{ mm s}^{-1}}{2.998 \cdot 10^{11} \text{ mm s}^{-1}} = 9.006 \cdot 10^{-9} \pm 6.7533 \cdot 10^{-9} \text{ eV} \quad (21)$$

2.2.2 Magnetic Field at the Core

The magnetic field at the core can be determined through the hyperfine structure splitting. The energy in the excited state can be expressed as

$$E = E_0 + B \left(\frac{\mu_g m_g}{I_g} - \frac{\mu_e m_e}{I_e} \right) \quad (22)$$

where the index g stands for ground state and e for excited state.

We observe a group of states with the same transition energy of 14.4 keV, that means a decay from $I = 3/2$ to $I = 1/2$. The selection rule $\Delta m = \pm 1$ allows six possible transitions. The resonances of these transitions can be found at different velocities, which gives us six equations

$$v_1 = c E + \frac{B}{E_0} (\mu_e - \mu_g) \quad (23a)$$

$$v_2 = c E + \frac{B}{E_0} \left(\frac{\mu_e}{3} - \mu_g \right) \quad (23b)$$

$$v_3 = c E + \frac{B}{E_0} \left(-\frac{\mu_e}{3} - \mu_g \right) \quad (23c)$$

$$v_4 = c E + \frac{B}{E_0} \left(\frac{\mu_e}{3} + \mu_g \right) \quad (23d)$$

$$v_5 = c E + \frac{B}{E_0} \left(-\frac{\mu_e}{3} + \mu_g \right) \quad (23e)$$

$$v_6 = c E + \frac{B}{E_0} (-\mu_e + \mu_g) \quad (23f)$$

Next we want to eliminate the unknown μ_e and E from the equations. Therefore we add or subtract different equations, for instance

$$v_4 - v_2 = v_5 - v_3 = \frac{2\mu_g Bc}{E_0} \quad (24)$$

The final form of B is now

$$B = \frac{E_0 \delta v}{2c\mu_g} \quad (25)$$

where we choose for δv the arithmetic mean of $v_4 - v_2$ and $v_5 - v_3$.

$$v_4 - v_2 = \pm 0.9844 \text{ mm s}^{-1} - \mp 3.2344 \text{ mm s}^{-1} = \pm 4.2188 \text{ mm s}^{-1} \quad (26)$$

$$v_5 - v_3 = \pm 3.3750 \text{ mm s}^{-1} - \mp 0.8438 \text{ mm s}^{-1} = \pm 4.2188 \text{ mm s}^{-1} \quad (27)$$

$$\implies \delta v = 4.2188 \text{ mm s}^{-1} \quad (28)$$

According to paragraph V. in [6] the value for μ_g is

$$\mu_g = 0.0903 \mu_k = 0.0903 \cdot 3.152 \cdot 10^{-8} \text{ eV T}^{-1} = 2.8463 \cdot 10^{-9} \text{ eV T}^{-1} \quad (29)$$

Plugging the results for δv and μ_g back into (25) we receive

$$B = \frac{14.4 \cdot 10^3 \text{ eV} \cdot 4.2188 \text{ mm s}^{-1}}{2 \cdot 2.998 \cdot 10^{11} \text{ mm s}^{-1} \cdot 2.8463 \cdot 10^{-9} \text{ eV T}^{-1}} = 35.5972 \pm 1.1863 \text{ T} \quad (30)$$

As uncertainty, again the channel width was assumed with $\Delta v = 0.1406 \text{ mm s}^{-1}$.

2.2.3 Magnetic Moment of the Excited State of ^{57}Fe

The magnetic moment of the excited state of ^{57}Fe can be determined by subtracting appropriate equations in (23). Doing so, we obtain

$$\mu_a = 3 \frac{v_2 - v_1}{\delta v} \mu_g = 0.1581 \mu_k \quad (31)$$

$$= \frac{3}{2} \frac{v_3 - v_1}{\delta v} \mu_g = 0.1579 \mu_k \quad (32)$$

$$= 3 \frac{v_3 - v_2}{\delta v} \mu_g = 0.1578 \mu_k \quad (33)$$

$$= 3 \frac{v_5 - v_4}{\delta v} \mu_g = 0.1581 \mu_k \quad (34)$$

$$= \frac{3}{2} \frac{v_6 - v_4}{\delta v} \mu_g = 0.1581 \mu_k \quad (35)$$

$$= 3 \frac{v_6 - v_5}{\delta v} \mu_g = 0.1487 \mu_k \quad (36)$$

$$\implies \mu_a = 0.1565 \mu_k \pm 0.0093 \mu_k \quad (37)$$

We used δv from the previous task and $\mu_g = 0.093 \mu_k$. The uncertainty was computed as the sum of the variance and the error from the channel width.

2.2.4 Velocity Calibration of the Mößbauer Spectrometer

The measurements are not exact due to the actual velocity of the Mößbauer drive differing from the adjusted velocity. A correcting factor can be computed by dividing the literature value by the sum of two outmost points.

$$f_{\text{gauge}} = \frac{\Delta v_{\text{lit}}}{v_6 - v_1} = \frac{10.6 \text{ mm s}^{-1}}{5.6250 \text{ mm s}^{-1} + 5.9062 \text{ mm s}^{-1}} = 0.9192 \quad (38)$$

This gauge factor has been taken into account for all further measurements.

2.3 Isomeric Shift and Electric Field Gradient in $\text{FeSO}_4 \cdot 7\text{H}_2\text{O}$

Procedure A Mößbauer spectrum is recorded at a drive velocity of 5 mm s^{-1} . From the shift of the symmetry axis of the spectrum with respect to drive velocity the isomeric shift can be computed, analogous to the one for ^{57}Fe . The electric field gradient of $\text{FeSO}_4 \cdot 7\text{H}_2\text{O}$ is determined using the energy level splitting, seen in the Mößbauer spectrum. This is then plugged in the equation for the quadrupole splitting, discussed in the theory part.

Experimental Setup The absorber-mount is placed in front of the Mößbauer drive. After the absorber-mount a scintillation counter is placed, attached to a photomultiplier and a preamp. The preamp is connected to the main amplifier, which is hooked up to a PC through a data-acquisition module. The data-acquisition module is also connected to the drive unit, where the velocity of the Mößbauer drive can be adjusted. For this second task we place a $\text{FeSO}_4 \cdot 7\text{H}_2\text{O}$ sample into the absorber-mount and toggle it to place the sample in the beam instead of the lead seal. Then we start the measurement for a period of 30 min with a drive velocity of 5 mm s^{-1} .

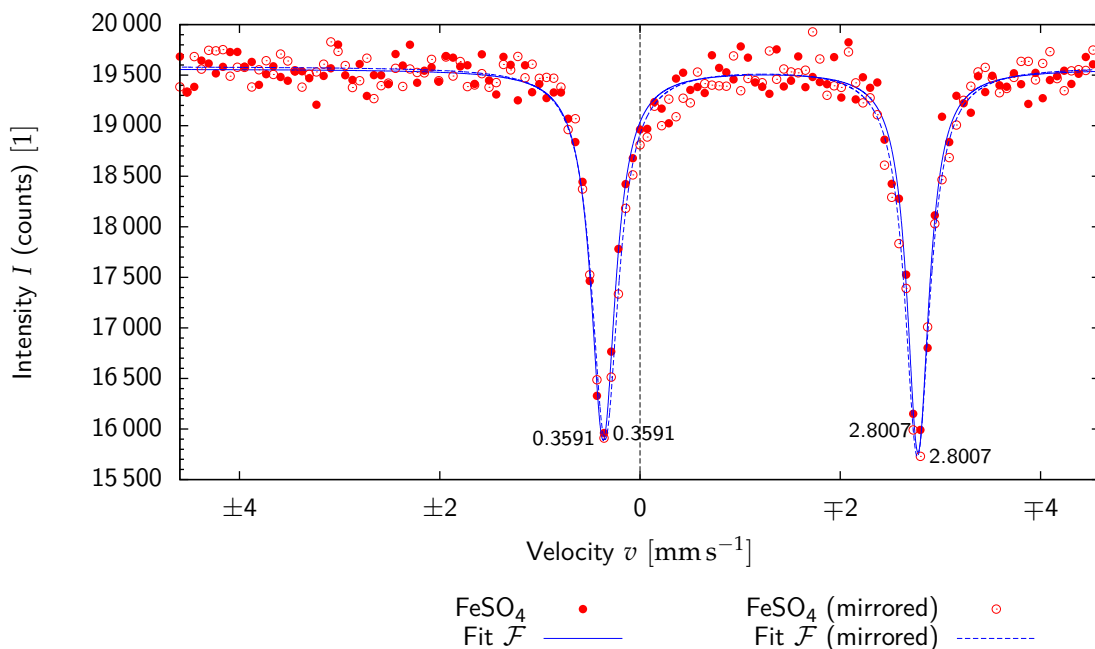


FIGURE 4: Transmission spectrum of $\text{FeSO}_4 \cdot 7\text{H}_2\text{O}$. The peaks have been annotated with the corresponding velocity of the Mößbauer drive.

2.3.1 Isomeric Shift

To compute the isomeric shift analogous to the one for ^{57}Fe , we need the shift of the symmetry axis with respect to the drive velocity. In this case it is the same for both, the solid and the dashed spectrum, with

$$\Delta v = \frac{2.4416\text{ mm s}^{-1}}{2} \quad (39)$$

Using the following equation the isomeric shift can be computed as

$$\Delta E = E_0 \frac{\Delta v}{c} = 14.4 \cdot 10^3\text{ eV} \frac{1.2208\text{ mm s}^{-1}}{2.998 \cdot 10^{11}\text{ mm s}^{-1}} = 5.8637 \cdot 10^{-8} \pm 0.677 \cdot 10^{-8}\text{ eV} \quad (40)$$

where we assumed the channel width of 0.1406 mm s^{-1} as error.

2.3.2 Computing the Electric Field Gradient

The recorded Mößbauer spectrum is plotted in figure 4. Two peaks are visible, which represent the two possible energy levels for the splitting. The associated difference in velocity is

$$\delta v = 3.4375 \text{ mm s}^{-1} \quad (41)$$

for both lines. In paragraph V. of [6] the value for the quadrupole moment is given as

$$Q = 0.29 \cdot 10^{-28} \text{ m}^2 \quad (42)$$

Plugging these into the equation of the quadrupole splitting we obtain

$$\begin{aligned} V_{zz} &= \frac{2 \delta v E_0}{e c Q} = \frac{2 \cdot 3.4375 \text{ mm s}^{-1} \cdot 14.4 \cdot 10^3 \text{ eV}}{1 \text{ eV V}^{-1} \cdot 2.998 \cdot 10^{11} \text{ mm s}^{-1} \cdot 0.29 \cdot 10^{-28} \text{ m}^2} \quad (43) \\ &= 1.1387 \cdot 10^{22} \pm 0.0466 \cdot 10^{22} \text{ V m}^{-2} \quad (44) \end{aligned}$$

2.4 Isomeric Shift of $\text{K}_4(\text{Fe}(\text{CN})_6) \cdot 3 \text{ H}_2\text{O}$

Procedure To determine the isomeric shift in $\text{K}_4(\text{Fe}(\text{CN})_6) \cdot 3 \text{ H}_2\text{O}$, a Mößbauer spectrum is recorded at a drive velocity 3 mm s^{-1} . From the shift of the symmetry axis the isomeric shift can be computed, analogous to the one for ^{57}Fe .

Experimental Setup The absorber-mount is placed in front of the Mößbauer drive. After the absorber-mount a scintillation counter is placed, attached to a photomultiplier and a preamp. The preamp is connected to the main amplifier, which is hooked up to a PC through a data-acquisition module. The data-acquisition module is also connected to the drive unit, where the velocity of the Mößbauer drive can be adjusted. For this second task we place a $\text{K}_4(\text{Fe}(\text{CN})_6) \cdot 3 \text{ H}_2\text{O}$ sample into the absorber-mount and toggle it to place the sample in the beam instead of the lead seal. Then we start the measurement for a period of 30 min with a drive velocity of 3 mm s^{-1} .

2.4.1 Computing the Isomeric Shift

In figure 5 we see the Mößbauer spectrum of $\text{K}_4(\text{Fe}(\text{CN})_6) \cdot 3 \text{ H}_2\text{O}$. The shift towards 0 is on average

$$\Delta v = -0.1078 \text{ mm s}^{-1} \quad (45)$$

Plugging this into equation (21) we receive

$$\Delta E = E_0 \frac{\Delta v}{c} = 14.4 \cdot 10^3 \text{ eV} \frac{-0.1078 \text{ mm s}^{-1}}{2.998 \cdot 10^{11} \text{ mm s}^{-1}} = -5.1730 \cdot 10^{-9} \text{ eV} \quad (46)$$

Assuming, that the error is of the magnitude of the channel width, we would get an error of $6.7677 \cdot 10^{-9} \text{ eV}$, which is larger than the value itself.

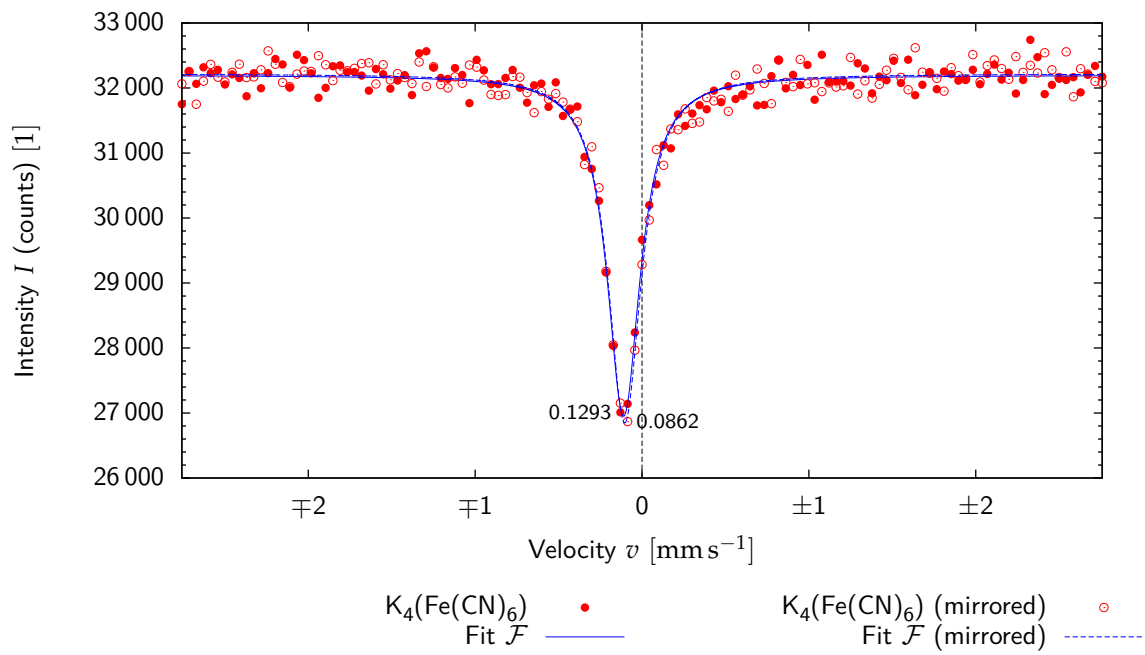


FIGURE 5: Transmission spectrum of $\text{K}_4(\text{Fe}(\text{CN})_6) \cdot 3 \text{H}_2\text{O}$. The peaks have been annotated with the corresponding velocity of the Mößbauer drive.

3 Summary

After a qualitative analysis of the spectrum of ^{57}Co , a group of properties was computed for ^{57}Fe from this spectrum. The isomeric shift was determined as

$$\Delta E = 9.006 \cdot 10^{-9} \pm 6.7533 \cdot 10^{-9} \text{ eV} \quad (47)$$

where

$$\Delta v = 0.1875 \text{ mm s}^{-1} \pm 0.1406 \text{ mm s}^{-1} \quad (48)$$

opposed to a literature value of

$$\Delta v_{\text{lit}} = 0.35 \text{ mm s}^{-1} \quad (49)$$

The magnetic field at the of the iron atom was calculated with

$$B = 35.5972 \pm 1.1863 \text{ T} \quad (50)$$

The magnetic moment of the excited state of ^{57}Fe has a value of

$$\mu_a = 0.1565 \mu_k \pm 0.0093 \mu_k \quad (51)$$

In the next part we obtained the isomeric shift and electric field gradient in $\text{FeSO}_4 \cdot 7 \text{H}_2\text{O}$. The isomeric shift is

$$\Delta E = 5.8637 \cdot 10^{-8} \pm 0.677 \cdot 10^{-8} \text{ eV} \quad (52)$$

with

$$\Delta v = -1.2208 \pm 0.1406 \text{ mm s}^{-1} \quad (53)$$

compared to the literature value

$$\Delta v_{\text{lit}} = 0.92 \text{ mm s}^{-1} \quad (54)$$

The electric field gradient could be computed as

$$V_{zz} = 1.1387 \cdot 10^{22} \pm 0.0466 \cdot 10^{22} \text{ V m}^{-2} \quad (55)$$

at a velocity shift of

$$\delta v = 3.4375 \text{ mm s}^{-1} \quad (56)$$

The documented value is

$$\delta v_{\text{lit}} = 3.19 \text{ mm s}^{-1} \quad (57)$$

which is very exact compared to the other deviations.

In the last part the isomeric shift in $\text{K}_4(\text{Fe}(\text{CN})_6) \cdot 3 \text{H}_2\text{O}$ was calculated. We obtained a value of

$$\Delta E = 5.1730 \cdot 10^{-9} \text{ eV} \quad (58)$$

and

$$\Delta v = 0.1078 \text{ mm s}^{-1} \quad (59)$$

The documented value is

$$\Delta v_{\text{lit}} = -0.39 \text{ mm s}^{-1} \quad (60)$$

List of Figures

1	Decay of ^{57}Co to the excited state of ^{57}Fe by electron capture. The γ -ray emission at the 14.4 keV level has a probability of about 10%. Other decay processes at that level occur by internal conversion. The transition energies were obtained from [1, p. 44, fig. 4.1]	4
2	Emission spectrum of ^{57}Co	9
3	Transmission spectrum of elemental iron. The peaks have been annotated with the corresponding velocity of the Mößbauer drive.	10
4	Transmission spectrum of $\text{FeSO}_4 \cdot 7\text{H}_2\text{O}$. The peaks have been annotated with the corresponding velocity of the Mößbauer drive.	13
5	Transmission spectrum of $\text{K}_4(\text{Fe}(\text{CN})_6) \cdot 3\text{H}_2\text{O}$. The peaks have been annotated with the corresponding velocity of the Mößbauer drive.	15

List of Tables

1	Comparison of the differences of the velocities compared between left and right side. 11
---	--

References

- [1] J. Bland. 'A Mössbauer Spectroscopy and Magnetometry Study of Magnetic Multilayers and Oxides'. PhD thesis. Oliver Lodge Laboratory, Department of Physics, University of Liverpool: University of Liverpool, Sept. 2002. URL: <http://www.cmp.liv.ac.uk/frink/thesis/thesis/node51.html>.
- [2] G. Blatter. *Quantenmechanik I*. 1. Aufl. ETH Zürich, 2005.
- [3] W. Demtröder. *Experimentalphysik 1: Mechanik und Wärme*. 5., überarb. u. aktual. Aufl. Springer Verlag, Mar. 2008.
- [4] H. Haken and H. C. Wolf. *Atom- und Quantenphysik*. 8., aktual. u. erw. Aufl. Springer Verlag, 2004.
- [5] W. T. of Radioactive Isotopes. *⁵⁷Co*. [Online; accessed 12-May-2013]. 1999. URL: <http://ie.lbl.gov/toi/nuclide.asp?iZA=270057>.
- [6] Universität Stuttgart (Hrsg.) *Physikalisches Praktikum II: Versuchsanleitung*. Universität Stuttgart. 2013.
- [7] H. Wegener. *Der Mössbauer-Effekt und seine Anwendungen in Physik und Chemie*. 2., erweiterte Auflage. Hochschultaschenbücher-Verlag, 1966.